A Tetravalent Bispecific Antibody Selectively Inhibits Diverse FGFR3 Oncogenic Variants

Yan Yang, Avvaru N. Suhasini, Zaoli Jiang, Nina Liu, Michael Rosconi, Bojie Zhang, Yinyin Li, Drew Dudgeon, Changhyun Seong, Steven Kim, Ashique Rafique, Tammy Huang, Sangram Bhosle, Pamela Krueger, Erica Ullman, William Olson, John C. Lin, Yang Shen, and Christopher Daly

ABSTRACT

The receptor tyrosine kinase FGFR3 is frequently mutated in bladder cancer and is a validated therapeutic target. Although pan-FGFR tyrosine kinase inhibitors (TKI) have shown clinical efficacy, toxicity and acquired resistance limit the benefit of these agents. While antibody-based therapeutics can offer superior selectivity than TKIs, conventional ligand-blocking antibodies are usually ineffective inhibitors of constitutively active receptor tyrosine kinases. Furthermore, the existence of multiple oncogenic variants of FGFR3 presents an additional challenge for antibody-mediated blockade. Here, we developed a tetravalent FGFR3×FGFR3 bispecific antibody that inhibited FGFR3 point mutants and fusion proteins more effectively than any of the conventional FGFR3 antibodies that we produced. Each arm of the bispecific antibody contacted two distinct epitopes of FGFR3 through a *cis* mode of binding. The antibody blocked dimerization of the most common FGFR3 oncogenic variant (S249C extracellular domain mutation) and inhibited the function of FGFR3 variants that are resistant to pan-FGFR TKIs. The antibody was highly effective in suppressing growth of FGFR3-driven tumor models, providing efficacy comparable to that of the FDA-approved TKI erdafitinib. Thus, this bispecific antibody may provide an effective approach for broad and highly selective inhibition of oncogenic FGFR3 variants.

Significance: Development of a bispecific antibody that broadly inhibits gain-of-function FGFR3 variants provides a therapeutic strategy to target tumors with oncogenic FGFR3 point mutations and fusions, a particularly difficult case for antibody blockade.

Introduction

Oncogenic alterations in FGFR3 are found in ~15% of muscle invasive bladder cancers (MIBC) and ~50% to 60% of non-MIBC (NMIBC; refs. 1–3). The most common FGFR3 alterations are extracellular point mutations that create an unpaired cysteine between immunoglobulin-like domains 2 and 3, leading to ligand-independent receptor dimerization (the FGFR3 S249C mutation accounts for ~60% of all FGFR3 mutations; refs. 4, 5). In addition, constitutive activation of FGFR3 can be driven by fusion with a coiled-coil domain (most commonly from the *TACC3* gene) that promotes dimerization (the fusion protein junctions are near the cytoplasmic C-terminus of FGFR3). FGFR3 fusions are less common than point mutations, occurring in ~2% of bladder cancers (6). Consistent with a role for FGFR3 as an oncogenic driver, the FDA-approved pan-FGFR tyrosine kinase inhibitor (TKI) erdafitinib provides a significant overall survival (OS) advantage versus chemotherapy in patients with metastatic urothelial cancer harboring FGFR3 point mutations or FGFR2/3 gene fusions (4, 7, 8).

Although pan-FGFR TKIs exhibit clinical efficacy, the blockade of multiple FGFR family members leads to significant toxicity, including hyperphosphatemia (as a result of FGFR1 inhibition), as well as gastrointestinal, nail, skin, and ocular toxicities (4, 7, 9). Thus, specific FGFR3-blocking antibodies have been explored as an alternative therapeutic class. For example, the fully human antibody R3Mab potently blocks the ligand binding to FGFR3 but only provides modest efficacy in preclinical tumor models driven by FGFR3 S249C or FGFR3-TACC3 fusion (10). This FGFR3 antibody (also known as B-701 or vofatamab) was tested as a monotherapy and in combination with docetaxel in patients with urothelial cancer harboring FGFR3 genetic alterations (11). In addition, vofatamab was tested in combination with pembrolizumab in both FGFR3 wild type and FGFR3-altered urothelial cancers (12). Although vofatamab showed some signs of activity (achieving response rates of 5% as monotherapy, 24% in combination with docetaxel, and 36% in combination with pembrolizumab), these clinical trials were terminated and the overall number of patients treated have remained small, making it difficult to draw definitive conclusions about efficacy.

Additionally, the diverse location of FGFR3 genetic alterations (ECD, juxta-membrane region, kinase domain, and C-terminal in-frame fusion) and the different mechanisms of receptor activation present a major obstacle to the generation of an FGFR3-blocking antibody that is effective against all variants. In this report, we describe the generation of a tetravalent, bispecific alternative-format antibody (R3-Altibody) that binds to two distinct epitopes on FGFR3. R3-Altibody, unlike any of our conventional antibodies, is highly effective against FGFR3 cysteine point mutations, FGFR3-TACC3 fusion, and TKI-resistant gatekeeper mutations. In FGFR3-

Regeneron Pharmaceuticals, Inc., Tarrytown, New York.

Corresponding Author: Yan Yang, Regeneron Pharmaceuticals, Inc., 777 Old Saw Mill River Road, Tarrytown, NY 10591. E-mail: yan.yang@regeneron.com

Cancer Res 2024;84:2169–80

doi: 10.1158/0008-5472.CAN-23-3195

driven tumor models, our antibody provides efficacy similar to that of the FDA-approved TKI erdafitinib. Thus, our antibody may provide a novel approach for the selective and potent inhibition of multiple FGFR3 oncogenic variants.

Materials and Methods

Antibody and reagents

Fully human antibodies against the hFGFR3b-ECD were generated in VelocImmune mice using methods described previously (13). cDNA encoding FGFR3×FGFR3 bispecific tetravalent antibody heavy chains and light chains were generated by DNA synthesis (Thermo Scientific) and cloned into pcDNA3.4 TOPO mammalian expression vector (Life Technologies). The linkers between single-chain variable fragment (scFv) light chain (VL) and heavy chain (VH) or scFv and fragment antigen-binding (Fab) were $(GGGS)_4$. Bispecific antibodies were produced by cotransfection of light chain and heavy chain expression vectors in Expi293F cells (Thermo Fisher Scientific). In-house version of comparator antibody was generated from published primary sequence (B701/Vofatamab, Patent WO2016/0243228A1) and were produced in CHO-K1 cells (ATCC) at Regeneron.

Antibodies against FGFR3 were obtained from Santa Cruz Biotechnology (RRID: AB_627596) or Cell Signaling Technology (RRID: AB_2246903). pMAPK (RRID: AB_2315112), MAPK (RRID: AB_390779), and actin (RRID: AB_2714189) antibodies were obtained from Cell Signaling Technology. Anti-phosphotyrosine pY100–agrose (RRID: AB_331231) was obtained from Thermo Fisher Scientific. AZD4547 and erdafitinib were obtained from Selleckchem. rhFGF1 and heparinases were purchased from R&D Systems. Heparin and cycloheximide were obtained from Sigma-Aldrich. Protease inhibitors and phosphatase inhibitors were obtained from Roche.

Cell lines were obtained from Sigma (UMUC14), ATCC (CHO-K1, RT4, FaDu), DSMZ (RT-112, BaF3), Takara (Lenti-X 293T), and Thermo Fisher Scientific (Expi293F). All cell lines tested negative for *Mycoplasma* by IDEXX IMPACT I PCR test.

Spheroid proliferation assay

Tumor cells were seeded in U-bottom low-attachment 96-well spheroid plate (Corning) in complete medium and cultured for 48 hours to allow spheroid formation. Tumor cell spheroids were treated with antibodies at the indicated concentration for 5 to 6 days and subjected to CellTiter-Glo 3D Cell Viability Assay (Promega). The luminescent signal was detected by using EnVision Plate Reader (PerkinElmer). The data were analyzed using Prism software (GraphPad). Cell proliferation was expressed as percentages of untreated controls.

FGFR3 dimerization, phosphorylation, and downstream signaling

For receptor dimerization assay, the cells were treated with the indicated antibodies for 3 hours. Equal amounts of cell lysates were analyzed by either reducing or nonreducing SDS-PAGE. Membranes were blotted with anti-FGFR3 primary antibody (Santa Cruz), developed with SuperSignal West Pico substrate (Pierce), and luminescence images were captured with a c300 imager (Azure Biosystems).

To test the effects of FGFR3 antibody on receptor phosphorylation and downstream signaling, the cells were serum starved overnight in the presence or absence of the indicated antibodies followed by ligand (human 100 ng/mL FGF1 and 10 μg/mL heparin) stimulation for 15 minutes at 37°C. Equal amounts of cell lysates were analyzed by using SDS-PAGE. Blots were incubated with pMAPK, MAPK, or actin antibody followed by incubation with horseradish peroxidase–conjugated secondary antibody. For FGFR3 phosphorylation, equal amounts of cell lysates were incubated with pY100 Sepharose beads overnight and nonspecific binding was removed by washing with lysis buffer. Immunoprecipitated proteins were analyzed by using reducing or nonreducing SDS-PAGE and blotted with FGFR3 antibody.

Growth inhibition of BaF3 cell line expressing FGFR3 mutants

cDNA-expressing FGFR3 (S249C, S248C, Y375C, V555M/L, S249C+ V555M/L) was synthesized and cloned into pLVX lentiviral vector (Thermo Fisher Scientific). Virus was generated by lipofectamine transfection of Lenti-X 293T cells using Lenti-X packaging single shots, following the manufacture's protocol (Clontech/Takara). Virus was concentrated using Lenti-X concentrator, and the titer was determined using the Lenti-X p24 Rapid Titer Kit (Clontech/Takara). BaF3 cells were transduced with the virus at ~0.3 multiplicity of infection. The expression of FGFR3 receptors was confirmed by FACS analysis and Western blot.

For the cell proliferation assays, engineered BaF3/hFGFR3 cells grown in complete medium were washed and plated in IL-3-free culture media ± 5 μg/mL heparin and 1 nmol/L human FGF1. The cells were plated out at 1×10^5 cells/well, into 96-well plates, followed by the addition of 1:3 serially diluted antibodies . After the addition of antibodies, the cells were incubated at 37°C for 72 hours, followed by the addition of CellTiter-Glo (Promega) reagent. The luminescent signal was detected by EnVision Plate Reader (PerkinElmer). The data were analyzed using Prism software (GraphPad).

Antibody epitope mapping by hydrogen deuterium exchange analysis

The hydrogen deuterium exchange (HDX) experiment was performed using a customized HDX automation system (NovaBioAssays) coupled to a Q Exactive HF mass spectrometer (Thermo Fisher Scientific). To initiate deuterium exchange, 10 μL of the protein sample (hFGFR3b-ECD alone or hFGFR3b-ECD mixed with FGFR3 Ab1, Ab3, R3-Altibody, or Ab4 at 2:1 ratio) was diluted with 90 μL PBS-D_2O buffer (10 mmol/L, pH 7.4) and incubated for 5 minutes. The reaction was quenched by adding 100 μL quenching buffer [0.5 mol/L Tris (2-carboxy-ethyl)-phosphine-HCl, 4 mol/L guanidine hydrochloride, pH 2.08]. The samples were then digested by online pepsin/protease XIII column (NovaBioAssays) at a flow rate of 100 μL/minute with 0.1% formic acid in water. Peptic peptides were trapped by an ACQUITY UPLC Peptide BEH C18 VanGuard Pre-column (2.0 mm × 5 mm) and further separated by using an ACQUITY UPLC Peptide BEH C18 column (2.0 mm × 50 mm). The eluted peptides were analyzed by using Q Exactive HF mass spectrometry in the LC-MS/MS or LC-MS mode.

The deuterium uptake percentage (D%) of individual peptides was calculated. Differences in deuterium uptake were calculated as ΔD% = D% of hFGFR3b-antibody − D% of hFGFR3b. The differences were considered significant if $|\Delta D| > 20\%$ (averaged from two replicates). The mass spectra of peptides showing significant differences were confirmed manually.

Asymmetric flow field–flow fraction coupled with multiangle light scattering and size exclusion chromatography coupled with multiangle light scattering analysis of R3-Altibody complex formation with FGFR3-ECD

R3-Altibody was combined with hFGFR3b-ECD at indicated ratios. All samples were incubated at ambient temperature for

2 hours and injected into an Eclipse DualTec A4F separation system coupled to an Agilent 1200 HPLC with DAWN laser light scattering instrument and an Optilab T-rEX differential refractometer detector (Wyatt Technology). The data were analyzed using ASTRA 7 software (Wyatt Technology).

To evaluate molecular weights and stoichiometries of N-scFv-Fab:hFGFR3b-ECD complex, N-scFv-Fab was combined with hFGFR3b-ECD to yield the molar ratio of 1:1 in 1× Dulbecco's Phosphate Buffered Saline (DPBS), pH 7.4. The samples were incubated at ambient temperature for 2 hours and maintained unfiltered at 4°C prior to injection into a BEH450 column (450 Å, 2.5 μm, 4.6 mm × 300 mm) coupled to a Waters (Milford) UPLC system equipped with a UV diode array detector, a Wyatt Technology microDAWN laser light scattering instrument, and an Optilab T-rEX differential refractive index detector connected in series. BSA was injected separately and included as a system suitability control.

Antibody inhibition of oncogenic FGFR3-driven signaling and tumor signaling growth

Tumor cells (5×10^6 UMUC14 or RT112 in 50% Matrigel) were implanted subcutaneously into the right flank of 6- to 8-week-old female SCID mice (Jackson Laboratory). Once tumors were established (~150–200 mm^3 in volume), the mice were randomized into treatment groups ($n = 7$–10 mice per group) and injected intraperitoneally twice per week with anti-FGFR3 antibodies or isotype control at indicated doses. Tumor volume was expressed in cubic millimeters using the formula: $V = 0.5 \times a \times b^2$, where a and b are the long and short diameters of the tumor, respectively. Tumor sizes were monitored twice weekly. All studies were approved by the Regeneron Institutional Animal Care and Use Committee. All data were analyzed using Prism software (GraphPad) and tumor sizes graphed as mean ± SEM. Tumor growth inhibition in squamous cell lung carcinoma PDX model expressing FGFR3 S249C was tested by using WuXi AppTec. The LU-0813 model was implanted into 6- to 8-week-old female BALB/c nude mice ($n = 7$ per group). Erdafitinib was dosed at 25 mg/kg via daily oral gavage. Ten to 13.3 mg/kg of antibodies were dosed by intraperitoneal injection twice weekly. Statistical analysis of difference in tumor volume among the groups was conducted on the data obtained on day 28. All data were analyzed using GraphPad Prism. Two-tailed t tests were performed and $P < 0.05$ was considered statistically significant.

Data availability

All data are available from the corresponding author upon reasonable request.

Results

FGFR3×FGFR3 antibody inhibits cell proliferation driven by FGFR3 S249C or FGFR3-TACC3 fusion

To identify antibodies capable of blocking multiple FGFR3 oncogenic variants, we generated fully human FGFR3 antibodies using VelocImmune mice (13). Antibodies were screened for specific binding to the FGFR3-ECD, inhibition of ligand binding, induction of receptor degradation, and inhibition of tumor cell growth. Although antibodies were identified that strongly inhibited the growth of UMUC14 urothelial carcinoma cells harboring FGFR3 S249C mutation (FGFR3 Ab1) or RT4 bladder cancer cells harboring FGFR3-TACC3 fusion (FGFR3 Ab4), we did not identify a conventional antibody that was a potent inhibitor of both FGFR3 variants (**Fig. 1A**). Similarly, a comparator antibody (COMP Ab—an in-house version of B-701/Vofatamab) significantly inhibited the growth of RT4 cells but had only a marginal effect on the growth of UMUC14 cells (**Fig. 1A**). Biacore analysis showed that Ab1 (the most effective inhibitor of UMUC14 cell growth) and Ab4 (the most effective inhibitor of RT4 cell growth) did not compete for binding to FGFR3 (Supplementary Fig. S1). Therefore, we tested whether the combination of these two antibodies could provide blocking activity that was superior to that of each antibody alone. The combination of Ab1 plus Ab4 was less effective than Ab1 in the FGFR3 S249C-expressing UMUC14 cells and was no more effective than Ab4 in the FGFR3-TACC3–expressing RT4 cells (Supplementary Fig. S2).

Since combining Ab1 and Ab4 did not provide the desired efficacy, we used a set of nine conventional FGFR3 antibodies to design and screen a panel of bispecific tetravalent Altibodies. The set of conventional antibodies consisting of Ab1 and Ab4 (our best blockers of oncogenic FGFR3) plus additional antibodies were selected on the basis of ligand blocking activity and specificity toward FGFR3b and 3c splicing variants (**Fig. 1B**; Supplementary Table S1). The Fab arms from Ab1 and Ab4 were linked at their N-termini to scFvs derived from eight other antibodies to generate a set of 16, 2 + 2 N-scFv molecules. In addition, Ab1 was linked at C-termini to scFvs from the eight other antibodies to generate a set of eight 2 + 2 C-scFv molecules. We screened candidates for their ability to inhibit growth of UMUC14 and RT4 tumor cells and identified a molecule that we refer to as R3-Altibody (consisting of anchored Fab arms from Ab1 linked to scFv from Ab3 in 2 + 2 N-scFv format) as our top candidate (**Fig. 1B**). Although Ab3 on its own did not inhibit the proliferation of either UMUC14 or RT4 cells, R3-Altibody inhibited UMUC14 cell proliferation more potently than Ab1 (R3-Altibody IC_{50} was 3- to 10-fold lower than Ab1 IC_{50}; **Fig. 1C**). In RT4 cells, R3-Altibody was significantly more effective than Ab1, inhibiting proliferation to the same extent as Ab4 (**Fig. 1C**). Finally, the combination of Ab1 plus Ab3 was less effective than R3-Altibody at inhibiting proliferation of UMUC14 and RT4 cells (**Fig. 1D**), indicating that the bispecific antibody is the most broadly effective blocker and the molecular configuration of R3-Altibody is essential for its activity.

R3-Altibody scFv-Fab arms form a *cis* complex with the FGFR3-ECD

To gain insight into the molecular interaction between R3-Altibody and FGFR3, we performed HDX epitope mapping, which revealed that the binding epitope for Ab1 is in immunoglobulin-like domain 3 (D3), whereas the epitope for Ab3 is in immunoglobulin-like domain 1 (D1; **Fig. 2A**; Supplementary Fig. S3). This is consistent with the observations that Ab1 binding is specific to the FGFR3b isoform (the alternative splicing that generates the 3b and 3c isoforms occurs in D3), whereas Ab3 binds to both FGFR3b and 3c isoforms with high affinity (D1 is identical in 3b and 3c; Supplementary Fig. S4). Biacore analysis showed that R3-Altibody binds to FGFR3b monomer with much higher affinity (KD: 0.56 nmol/L) than Ab1 (2.6 nmol/L) or Ab3 (54 nmol/L; Supplementary Fig. S4), suggesting that both the D1 and D3 epitopes of monomeric FGFR3-ECD are engaged by the pre-captured R3-Altibody.

To further investigate the nature of the R3-Altibody interaction with FGFR3, we performed asymmetric flow field–flow fraction coupled with multiangle light scattering (A4F-MALS) analysis of the complex formed between R3-Altibody and monomeric FGFR3b-ECD. When combined at equimolar binding site ratio, R3-Altibody (1 μmol/L) and FGFR3b-ECD (2 μmol/L) form a complex (~327–329 kDa) at 1:2 stoichiometry with no sign of larger complexes (**Fig. 2B**, left, orange trace). When combined at varying molar ratios with excess of R3-Altibody (3:2) or

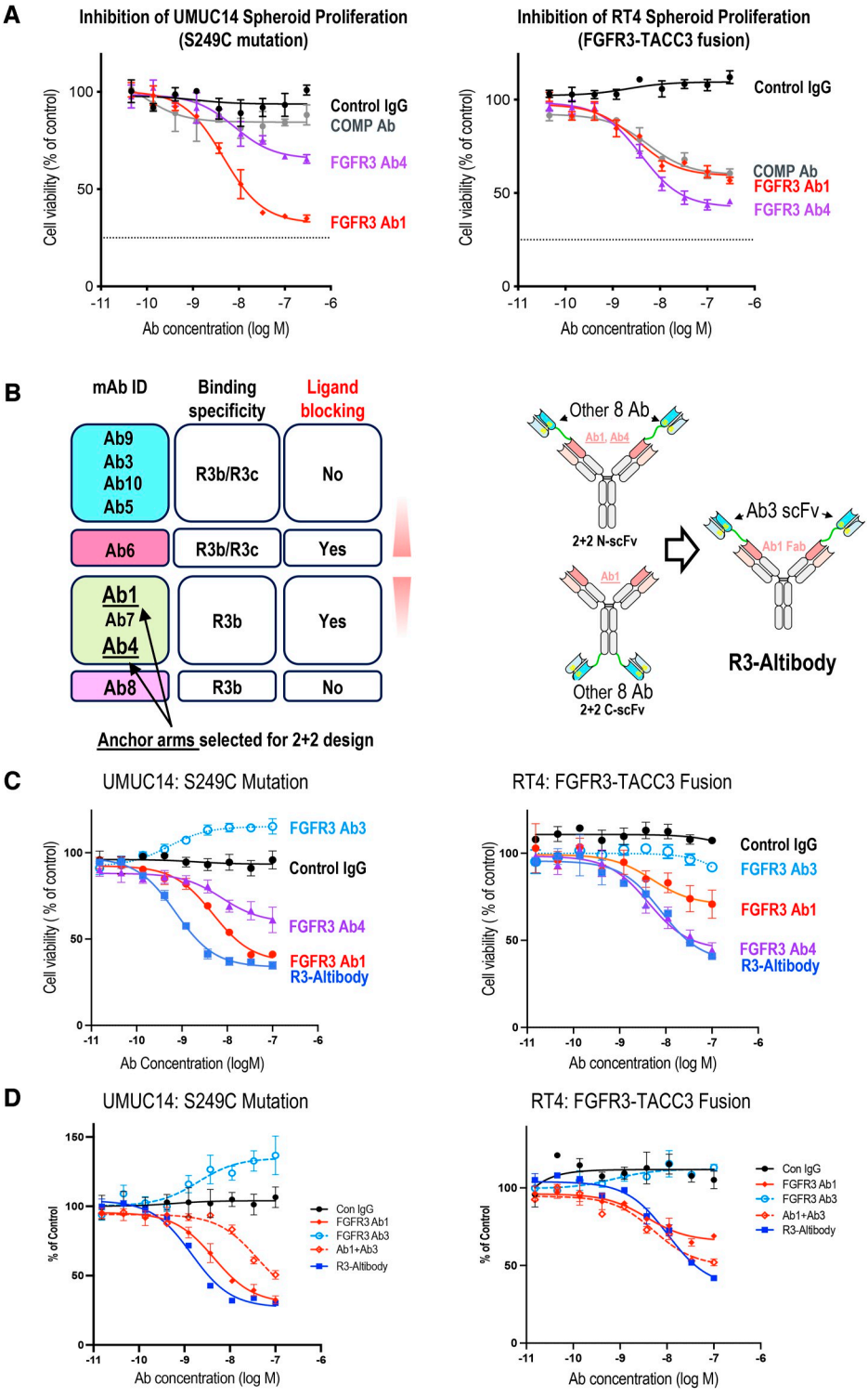

Figure 1.

R3-Altibody inhibits cell proliferation driven by FGFR3 S249C or FGFR3-TACC3 fusion. **A,** Effect of conventional FGFR3 antibodies on proliferation of urothelial carcinoma cells expressing FGFR3 S249C variant (UMUC14; left) or FGFR3-TACC3 fusion (RT4; right). Cell viability is expressed as percentage of untreated control and plotted as mean ± SEM. Assays were performed in triplicates. Dotted line indicates baseline cell viability prior to antibody dosing. **B,** Design of bispecific tetravalent FGFR3×FGFR3 antibodies. Nine FGFR3 antibodies with diverse characteristics (see Results for details) were selected for pairing. The Fab arms from Ab1 and Ab4 (our best blockers of oncogenic FGFR3) were linked at their N-termini to scFv derived from the eight other antibodies to generate a series of 16, 2 + 2 N-scFv molecules. In addition, the Fab arms from Ab1 were linked at their C-termini to scFvs from the eight other antibodies to generate a set of eight 2 + 2 C-scFv molecules. Functional screening identified R3-Altibody, which consists of anchored Fab arms from Ab1 linked to scFvs from Ab3 in 2 + 2 N-scFv format, as our lead candidate. **C,** The effect of conventional FGFR3 antibodies and R3-Altibody on proliferation of urothelial carcinoma cells expressing FGFR3 S249C variant (UMUC14; left) or FGFR3-TACC3 fusion (RT4; right). **D,** The effect of conventional FGFR3 antibodies, the combination of conventional antibodies Ab1 + Ab3, and R3-Altibody on proliferation of urothelial carcinoma cells expressing FGFR3 S249C variant (UMUC14; left) or FGFR3-TACC3 fusion (RT4; right).

FGFR3b-ECD (1:6), complexes at stoichiometries of 1:1 and 1:2 were the predominant species in solution and little to no higher-order complexes were detected under any condition tested (Supplementary Fig. S7). All together, these data suggest that each R3-Altibody engages at most two FGFR3b-ECD molecules, an interaction that could occur in either *cis* or *trans* mode, as depicted in **Fig. 2B** (left). To further deconvolute the binding mode, a single-arm scFv-Fab fragment of R3-Altibody was generated and mixed with FGFR3b-ECD, followed by size exclusion chromatography coupled with multiangle light scattering (SEC_MALS) analysis to assess complex formation. Formation of a 1:1 complex would

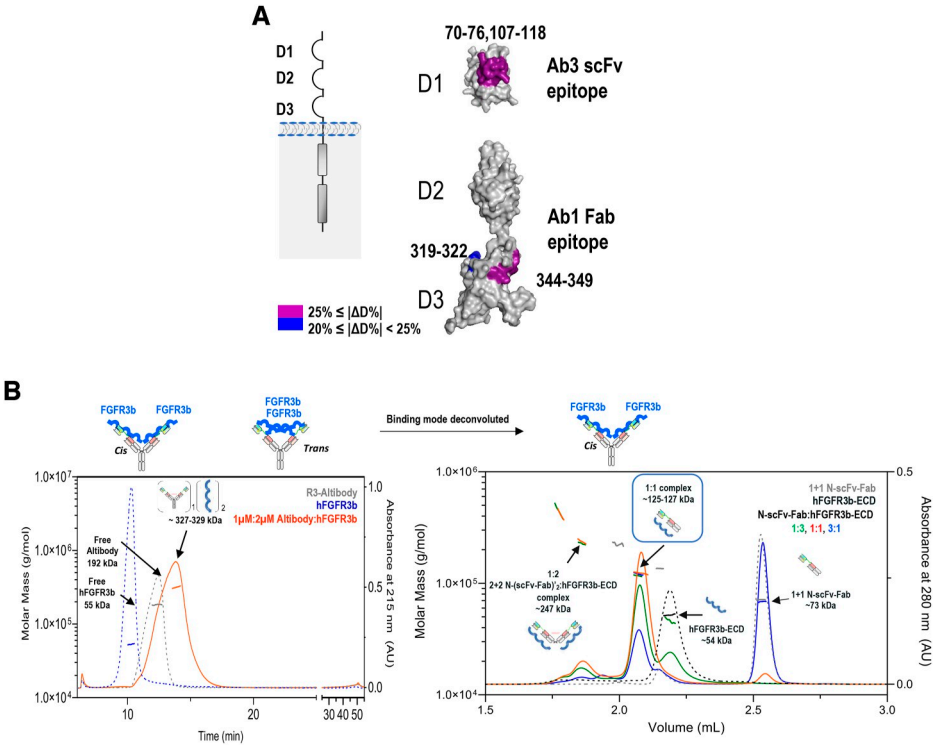

Figure 2.

The bispecific arms of R3-Altibody form *cis* complexes with FGFR3-ECD. **A,** HDX epitope mapping shows that Ab1 (Fab component of R3-Altibody) interacts with Ig-like domain 3, whereas Ab3 (N-term scFv component of R3-Altibody) interacts with Ig-like domain 1. Magenta, peptides that showed differences in deuterium uptake ΔD% ≥ 25%; blue, 25% >ΔD ≥ 20%. Structure of FGFR3 D2–D3 was adopted from PDB 1RY7, model of FGFR3 D1 was adopted from AlphaFold structure prediction (AF-P22607-F1-model_v4). **B,** R3-Altibody predominantly forms a 1:2 complex (calculated molecular weight 302 kDa) with monomeric FGFR3b-ECD when mixed at 1:2 μmol/L ratio (left). The molar masses of free FGFR3-ECD, R3-Altibody, and R3-Altibody in complex with FGFR3b-ECD were determined by A4F-MALS. The experimentally determined molar masses are indicated by horizon lines. Left, two models of the 1:2 complex are depicted as *cis* vs. *trans* binding. Right, the molar masses of the free FGFR3-ECD, scFv-Fab arm from R3-Altibody, and the scFv-Fab arm in complex with FGFR3b-ECD were determined by SEC-MALS. The chromatograms show traces representing scFv-Fab:hFGFR3b-ECD mixed at ratios of 1:3 (green), 1:1 (red), and 3:1 (blue). Molecular mass and pictogram of free scFv-Fab, FGFR3b-ECD, and the complex of scFv-Fab bound to FGFR3-ECD are shown above the corresponding peaks. The minor species of ~247 kDa is consistent with a 1:2 complex (in *cis* mode) between residual unreduced 2 + 2 $(scFv\text{-}Fab')_2$ in our preparation and FGFR3b-ECD. (**A,** Created with PyMOL.)

be consistent with a *cis* mode of binding, whereas a 2:2 complex would be consistent with a *trans* mode of binding. At 1:3, 1:1, and 3:1 mixing ratios, the predominant species (molar mass of ~125–127 kDa) is consistent with a 1:1 scFv-Fab:FGFR3b-ECD complex, suggesting a *cis* mode of binding (**Fig. 2B**, right). We do observe a minor species of ~247 kDa that is consistent with a 1:2 complex (in *cis* mode) between residual unreduced 2 + 2 $(scFv\text{-}Fab')_2$ in our preparation and FGFR3b-ECD.

R3-Altibody inhibits the function of oncogenic FGFR3 S249C by blocking heparin-dependent dimerization

It has been reported that FGFR3 receptors with extracellular point mutations like S249C form intermolecular disulfide bonds, leading to ligand-independent signaling. Inhibition of S249C signaling was not due to antibody-induced receptor degradation as R3-Altibody treatment did not change the receptor level (Supplementary Fig. S5). Previously Qing and colleagues (10) reported that the FGFR3 antibody R3Mab is capable of inhibiting dimerization of FGFR3 S249C. We therefore tested the effect of R3-Altibody on the formation of covalent FGFR3 dimers in UMUC14 cells. Nonreducing SDS-PAGE analysis showed that both R3-Altibody and Ab1 strongly inhibit dimer formation, Ab4 and COMP Ab have a partial effect and Ab3 has no effect (**Fig. 3A**; Supplementary Fig. S6). The relative effects of the antibodies on FGFR3 S249C dimer formation correlate well with their ability to inhibit the proliferation of UMUC14 cells (**Fig. 1A** and **C**), suggesting that inhibition of dimerization is an important component of the inhibitory action of R3-Altibody on FGFR3 S249C signaling. The combination of the parental antibodies for R3-Altibody, Ab1 plus Ab3, did not achieve the same level of dimer inhibition as R3-Altibody (**Fig. 3A**), indicating that the molecular configuration of R3-Altibody is required for its activity. Next, we investigated whether R3-Altibody prevents FGFR3 S249C dimer formation or promotes disassembly of existing dimers. To address this question, we treated FaDu cells engineered to express FGFR3 S249C with cycloheximide to prevent the synthesis of new FGFR3 S249C monomers, resulting in the accumulation of dimeric FGFR3 (**Fig. 3B**). The cells were then treated with R3-Altibody for an additional 4 hours (in the continued presence of cycloheximide). The addition of R3-Altibody did not result in disassembly of FGFR3 dimers to monomeric form (**Fig. 3B**), suggesting that R3-Altibody prevents monomeric FGFR3 S249C from forming dimers rather than enhancing dimer breakdown (**Fig. 3C**).

Consistent with the fact that FGFR dimerization is required for receptor autophosphorylation, dimeric FGFR3 S249C expressed in

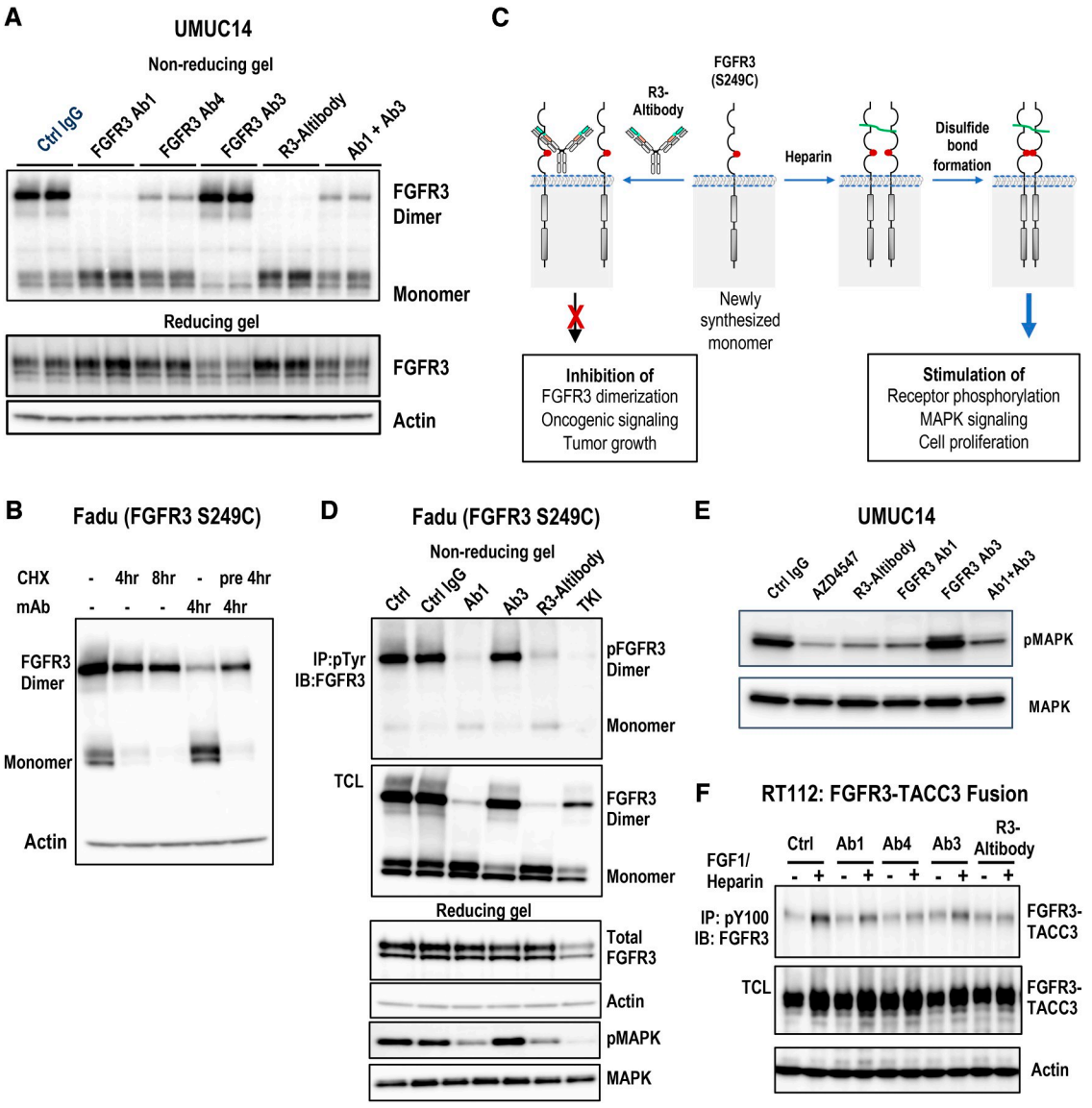

Figure 3.

R3-Altibody inhibits dimerization and activation of FGFR3 oncogenic variants. **A,** UMUC14 cells were treated with the indicated antibodies at 33 nmol/L for 3 hours (the Ab1 + Ab3 group was treated with 33 nmol/L of each antibody). The levels of FGFR3 covalent dimer vs. monomer were determined by nonreducing SDS-PAGE, followed by Western blot. The total FGFR3 levels were determined by reducing SDS-PAGE, followed by Western blotting. Duplicates of the samples are shown in the figure. **B,** FaDu cells stably expressing FGFR3 S249C were treated with 50 μg/mL cycloheximide (CHX) for 4 or 8 hours, 100 nmol/L of R3-Altibody for 4 hours, or with cycloheximide pretreatment for 4 hours, followed by R3-Altibody for an additional 4 hours. The levels of FGFR3 dimer vs. monomer were determined as described above. **C,** The model for the effect of R3-Altibody on dimerization of FGFR3 S249C. See text for details. **D,** FaDu cells stably expressing FGFR3 S249C were serum starved overnight in the presence of the indicated antibodies (300 nmol/L). Cell lysates were subjected to immunoprecipitation with antiphosphotyrosine antibody, followed by nonreducing SDS-PAGE and Western bloting to determine the levels of phosphorylated FGFR3 dimer and monomer. Total cell lysates (TCL) were analyzed by nonreducing SDS-PAGE and Western blotting to determine the total levels of FGFR3 dimer and monomer. Whole cell lysates were analyzed under reducing conditions to determine levels of total FGFR3, actin, pMAPK, and total MAPK. **E,** UMUC14 cells were serum starved overnight in the presence of the indicated antibodies (100 nmol/L). Cell lysates were analyzed by Western blot for pMAPK and total MAPK. **F,** RT112 cells that endogenously express FGFR3-TACC3 fusion protein were starved overnight in the presence of the indicated antibodies (100 nmol/L). FGF1 (100 ng/mL) and heparin (5 μg/mL) were then added to the cells for 15 minutes. Cell lysates were analyzed for phospho-FGFR3-TACC3 by immunoprecipitation/Western blotting as described above. Total cell lysates were analyzed for total FGFR3-TACC3 and actin loading control by Western blot.

FaDu cells is tyrosine phosphorylated, whereas minimal tyrosine phosphorylation is associated with monomeric FGFR3 (**Fig. 3D**). Both R3-Altibody and Ab1 treatment strongly inhibited FGFR3 S249C dimerization (consistent with the data from UMUC14 cells), as well as receptor phosphorylation and downstream MAPK signaling (**Fig. 3D**). The pan-FGFR TKI AZD4547 binds to the FGFR3

kinase domain and blocks enzymatic activity, thus it inhibits receptor phosphorylation but has a relatively modest impact on the fraction of FGFR3 that is dimeric (**Fig. 3D**). These experiments reveal that R3-Altibody achieves potent blockade of oncogenic FGFR3 S249C signaling through inhibition of FGFR3 dimerization. Consistent with their ability to inhibit FGFR3 S249C dimerization and phosphorylation, R3-Altibody and Ab1 treatment inhibited phosphorylation of MAP kinase (a major effector of FGFR3 signaling) in UMUC14 cells to roughly the same extent as AZD4547 (**Fig. 3E**). Finally, in RT112 cells endogenously expressing FGFR3-TACC3 fusion protein, R3-Altibody completely attenuated FGF1-/heparin-stimulated phosphorylation of FGFR3-TACC3 (**Fig. 3F**).

In FaDu head and neck cancer cells engineered to express FGFR3 S249C, ~70% of FGFR3 exists as a dimer (similar to UMUC14 cells that endogenously express FGFR3 S249C; **Fig. 3A** and **B**). Interestingly, when FGFR3 S249C was expressed in BaF3 cells, which do not produce heparan sulfate, the levels of FGFR3 dimer were significantly lower (~6%; **Fig. 4A**). In BaF3 cells, FGFR3 S249C dimerization was not enhanced by FGF1 treatment alone, consistent with prior reports that FGFR3 S249C dimerization is FGF1 independent (14). On the contrary, heparin treatment alone or in combination with FGF1 led to a marked increase of FGFR3 dimerization (**Fig. 4A**). Conversely, the treatment of UMUC14 cells with heparinase for 8 hours led to a marked decrease of covalent FGFR3 dimer formation, confirming that heparin is required for the disulfide bond formation between S249C monomers (**Fig. 4B**). Decreased receptor dimerization in the presence of heparinase also led to lower MAPK phosphorylation. Consistent with these findings, heparin, but not FGF1 alone, increased proliferation of BaF3 FGFR3 S249C cells in a dose-dependent manner (**Fig. 4C**). Finally, R3-Altibody was able to significantly inhibit heparin- or heparin/FGF1-induced FGFR3 dimerization and phosphorylation, as well as MAPK phosphorylation (**Fig. 4D**) and BaF3 cell proliferation (**Fig. 4E**).

R3-Altibody is highly effective in FGFR3-driven tumor models

We next assessed the efficacy of our FGFR3 antibodies in tumor xenograft models. Both R3-Altibody and Ab1 promoted significant regression of established UMUC14 tumors (FGFR3 S249C dependent) at doses of 3 to 4 mg/kg (**Fig. 5A**). Tumor growth inhibition by R3-Altibody and Ab1 was sustained for >20 days after treatment discontinuation (Supplementary Fig. S8). By contrast, Ab4 (our most effective inhibitor of FGFR3-TACC3–dependent RT4 cells) and the comparator FGFR3 antibody (COMP Ab) only provided modest tumor growth delay, even at 10 mg/kg, consistent with the relatively weak effects of these antibodies on growth of UMUC14 cells *in vitro*. COMP Ab was less effective than Ab1 and R3-Altibody despite its high binding affinity and ligand-blocking activity (Supplementary Fig. S6; ref. 10). The crystal structure of COMP Ab in complex with FGFR3-ECD revealed that the COMP Ab epitope is located predominantly in D2, different from Ab1 (D3) and R3-Altibody (D1/D3), suggesting that the ability to potently block FGFR3 S249C signaling requires both optimal epitope(s) and high affinity. Consistent with our *in vitro* tumor cell growth data, R3-Altibody at a suboptimal dose was more effective than its parental antibodies alone or in combination (**Fig. 5B**; Supplementary Fig. S8). Importantly, pharmacokinetic analysis (see Materials and Methods for details) showed that after a single administration, comparable serum levels of the R3-Altibody Fab component and scFv component were detected, indicating that R3-Altibody maintains its integrity *in vivo* for at least 30 days post administration (Supplementary Fig. S9). Consistent with its strong effect on UMUC14 tumor growth, R3-Altibody at 5 mg/kg markedly inhibited MAPK phosphorylation in tumors at 48 and 72 hours following administration (**Fig. 5C**), indicating a strong blockade of FGFR3 S249C signaling. The effect of R3-Altibody on MAPK phosphorylation was at least as strong as that of the maximally effective dose (25 mg/kg, once per day) of pan-FGFR TKI AZD4547.

We next tested the ability of R3-Altibody to inhibit the growth of a patient-derived lung squamous cell carcinoma model LU-0813 that harbors an FGFR3 S249C mutation. Both Ab1 and R3-Altibody strongly inhibited tumor growth, to approximately the same extent as the FDA-approved pan-FGFR TKI erdafitinib (**Fig. 5D**). Although FGFR3 genetic alterations in lung cancer are relatively rare, our data show that R3-Altibody provides strong anti-tumor activity in FGFR3-driven models that represent multiple cancer lineages.

Finally, in the RT112 xenograft model, which expresses the FGFR3-TACC3 fusion, both Ab4 and R3-Altibody significantly inhibited tumor growth, providing efficacy that was ~25% better than that of the parental Ab1 (**Fig. 5E**) and comparable to that of erdafitinib (Supplementary Fig. S10A). Similar to the UMUC14 model, COMP Ab was relatively ineffective in the RT112 model, as previously reported (10, 15). Interestingly, the partial response of RT112 tumors to R3-Altibody might be explained by the finding that EGFR signaling limits the sensitivity of RT112 cells to FGFR3 inhibition (16), rather than resulting from a failure of R3-Altibody to effectively block FGFR3-TACC3 signaling.

In summary, R3-Altibody demonstrates potent efficacy (superior to our conventional antibodies and to COMP Ab) in tumor models harboring FGFR3 S249C mutation or FGFR3-TACC3 fusion. In addition, although R3-Altibody (and Ab1) bind to murine FGFR3 with high affinity, no significant body weight loss (Supplementary Fig. S10B) or other gross abnormalities were observed in our studies, indicating that these antibodies are well tolerated in mice.

R3-Altibody potently inhibits cell proliferation driven by FGFR TKI-resistant gatekeeper mutations

Acquired resistance to FGFR TKIs has been reported and is frequently associated with secondary mutations in the kinase domain (17, 18). One of the resistance mutation hotspots that seems to drive disease progression is the gatekeeper mutation V555M/L. To test the efficacy of our FGFR3 antibodies in the context of TKI resistance mutations, we generated BaF3 cell lines expressing FGFR3 S249C with or without the gatekeeper mutations V557M or V557L. Since FGF1/heparin treatment stimulated phosphorylation of the mutant receptors in BaF3 cells (Supplementary Fig. S11), we performed the cell growth assays in the presence of FGF1/heparin. The pan-FGFR TKIs AZD4547 and erdafitinib potently inhibited the growth of BaF3 cells expressing FGFR3 S249C (IC_{50} 9.9 and 1.2 nmol/L, respectively; **Fig. 4D**) but were ineffective in cells expressing FGFR3 that contained V557M/L mutation alone or together with the S249C mutation (**Fig. 6A**). By contrast, both R3-Altibody and Ab1 were able to strongly inhibit the growth of BaF3 cells expressing the double mutant FGFR3 (S249C plus V557M or L).

Consistent with these effects on cell growth, R3-Altibody almost completely inhibited dimerization and phosphorylation of double

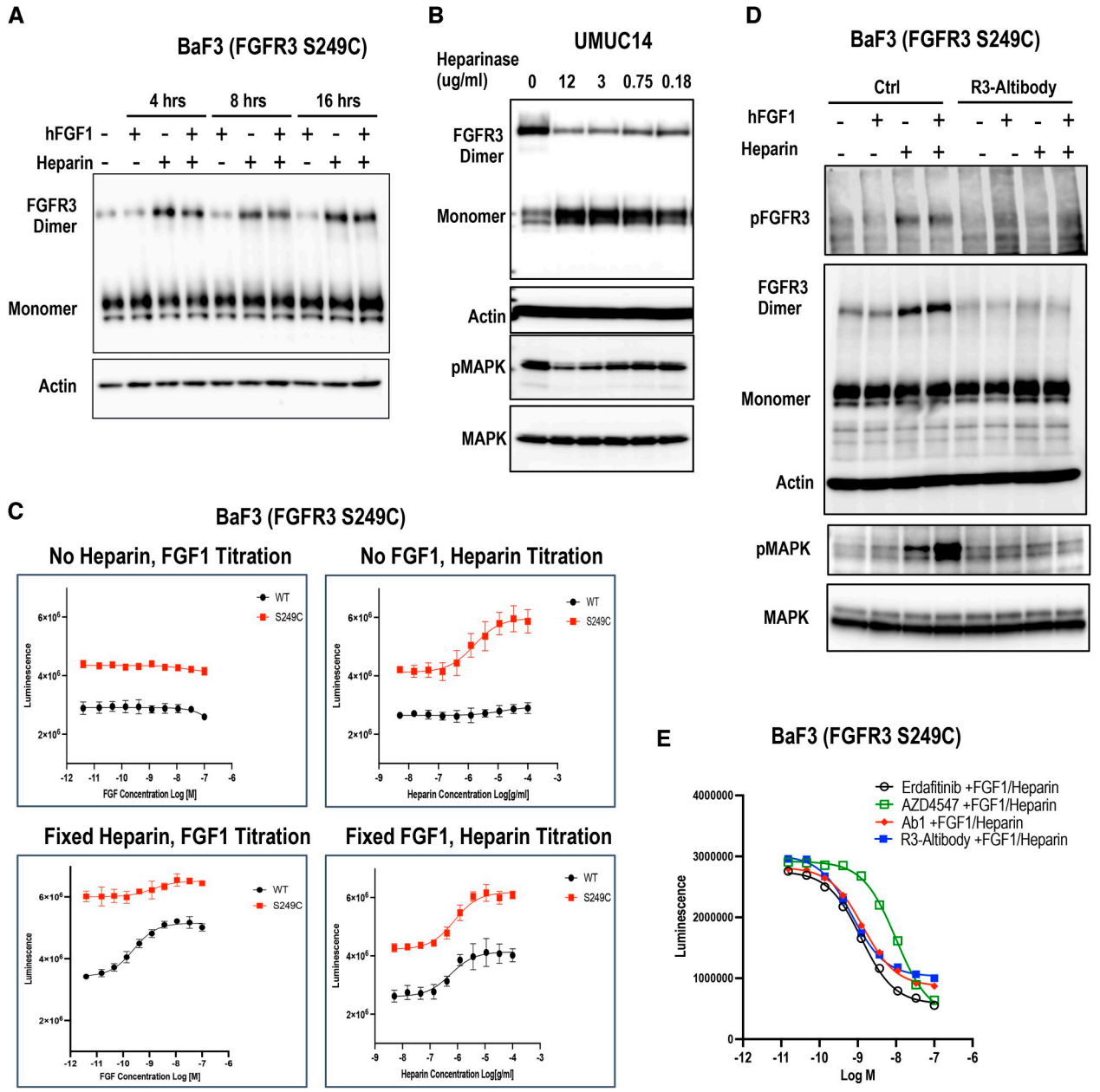

Figure 4.

Signaling by FGFR3 S249C is ligand independent but heparin dependent. **A,** BaF3 cells stably expressing FGFR3 S249C were treated with 100 nmol/L FGF1, 10 μg/mL heparin or hFGF1 + heparin for 4, 8, or 16 hours. The levels of FGFR3 covalent dimer vs. monomer were determined by nonreducing SDS-PAGE, followed by Western blot. The levels of total actin were determined by Western blot. **B,** UMUC14 cells were treated with the indicated concentrations of heparinase for 8 hours and cell lysates were analyzed for the levels of FGFR3 dimer vs. monomer, pMAPK, and total MAPK by Western blot. **C,** BaF3 cells expressing FGFR3 S249C were cultured for 72 hours in the presence of the indicated concentrations of FGF1 alone (top left), heparin (top right), increasing concentrations of FGF1 in the presence of 5 μg/mL heparin (bottom left), or increasing concentrations of heparin in the presence of 1 nmol/L FGF1 (bottom right). Cell viability was quantitated and mean luminescence intensity ± SEM are shown. Assays were performed in triplicates. **D,** BaF3 cells stably expressing FGFR3 S249C were serum starved overnight in the absence or presence of 100 nmol/L R3-Altibody. The cells were then treated with heparin alone, FGF1 alone, or FGF1 + heparin for 15 minutes. The levels of FGFR3 dimer vs. monomer, pFGFR3, pMAPK, and total MAPK were determined by Western blot. **E,** The effects of R3-Altibody, Ab1, AZD4547, and erdafitinib on proliferation of BaF3 cells expressing FGFR3 S249C were determined as described in **C**.

mutant FGFR3 receptors (S249C/V557M or L) and downstream MAPK signaling (**Fig. 6B**). By contrast, AZD4547 treatment resulted in only a weak/partial inhibition of FGFR3 double mutant phosphorylation and had no effect on MAPK phosphorylation. Because secondary FGFR3 kinase domain mutations seem to be a major mechanism of acquired resistance to FGFR inhibitors (17),

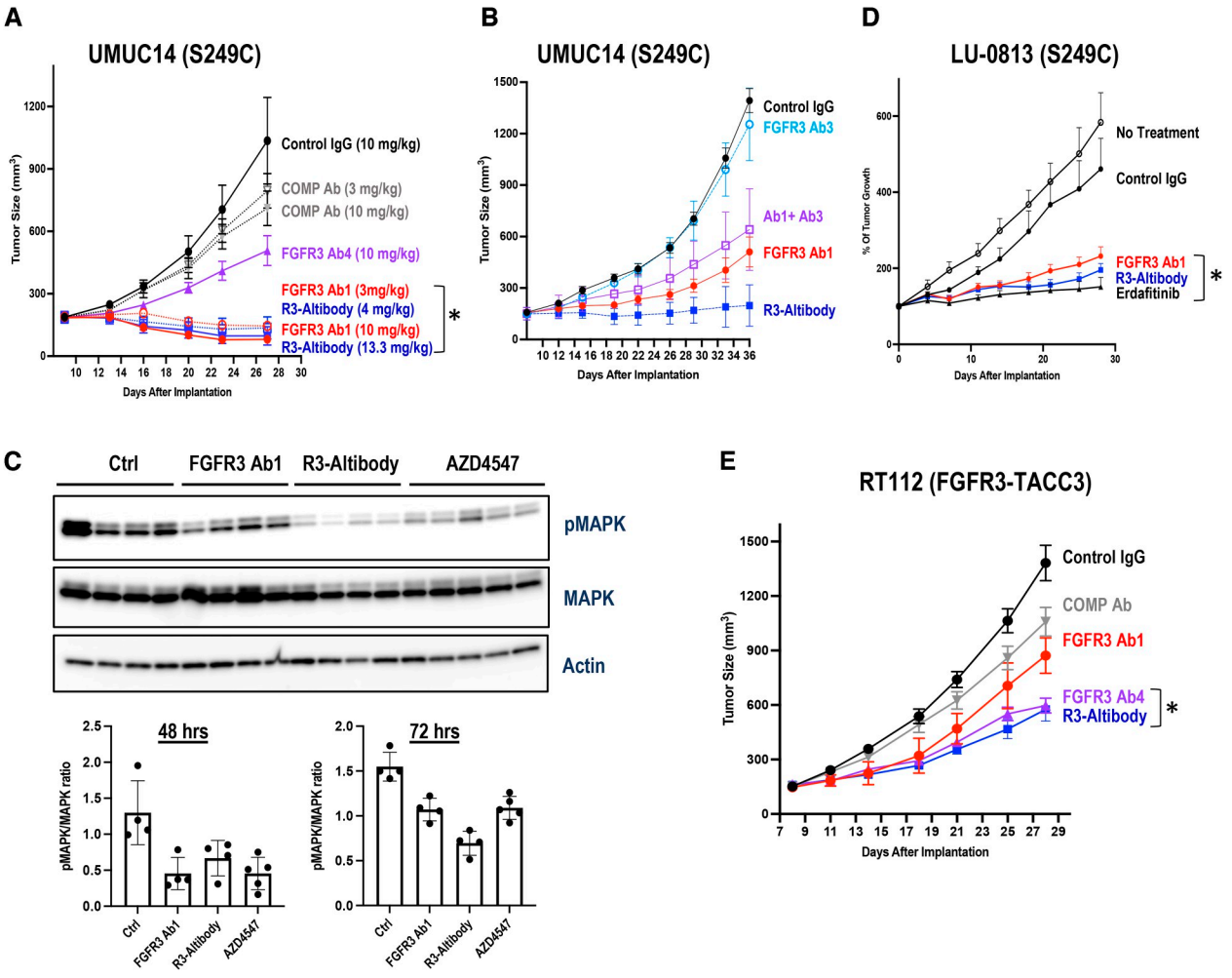

Figure 5.

R3-Altibody is highly effective in FGFR3-driven tumor models. SCID mice bearing established tumors were randomized and treated with the indicated antibodies. Line graphs depict the average tumor volumes ± SEM for each group. **A,** Mice bearing UMUC14 tumors were treated twice per week with the indicated antibodies ($n = 10$ per group). **B,** Mice bearing UMUC14 tumors were treated twice per week with FGFR3 Ab1 and Ab3 at 2 mg/kg, R3-Altibody at 2.66 mg/kg, or the combination of FGFR3 Ab1 + Ab3 at 2 mg/kg each ($n = 10$ per group). **C,** Mice bearing UMUC14 tumors were treated once with FGFR3 Ab1 (5 mg/kg) or R3-Altibody (6.65 mg/kg) or daily with AZD4547 (25 mg/kg). Tumors were collected at 48 or 72 hours after treatment. Tumor lysates were prepared, and the levels of pMAPK, MAPK, and actin were determined by Western blot. The bar graph depicts the ratio of pMAPK/MAPK for each group ($n = 4$–5; mean ± SEM). **D,** Mice bearing patient-derived LU-0813 lung squamous cell carcinomas (FGFR3 S249C) were either untreated or treated with the indicated agents. Control antibody and FGFR3 Ab1 were administered twice per week at 10 mg/kg. R3-Altibody was given twice per week at 13.3 mg/kg. Erdafitinib was administered daily by oral gavage at 25 mg/kg ($n = 7$ per group). **E,** Mice bearing established RT112 tumors (FGFR3-TACC3) were treated twice per week at 15 mg/kg with the indicated antibodies ($n = 10$ per group), except for R3-Altibody, which was administered at 20 mg/kg (molar equivalent). A two-tailed t test was performed to compare tumor volume among the control IgG group and treatment groups. *, $P < 0.05$.

the ability of R3-Altibody to inhibit the function of FGFR3 harboring gatekeeper mutations is a very attractive feature for a clinical candidate.

Discussion

In this report, we characterize the properties of a tetravalent bispecific FGFR3×FGFR3 Altibody that, unlike any of the conventional antibodies that we generated, is an effective inhibitor of multiple FGFR3 oncogenic variants (**Figs. 5** and **6**; Supplementary Fig. S12). R3-Altibody shows strong efficacy in tumor models driven by FGFR3 S249C or by FGFR3-TACC3 fusion, outperforming our version of vofatamab, a conventional FGFR3 blocking antibody that was previously in clinical development. In addition, R3-Altibody effectively blocks signaling by TKI-resistant FGFR3 variants that harbor gatekeeper mutations. Our findings highlight the therapeutic potential of R3-Altibody and support the general conclusion that the activity of bispecific antibodies can be distinct from a mixture of their two parental antibodies.

In addition to the implications for FGFR3-targeted therapy, our data shed light on the mechanisms that control signaling by the most common FGFR3 oncogenic variants. The ECD point

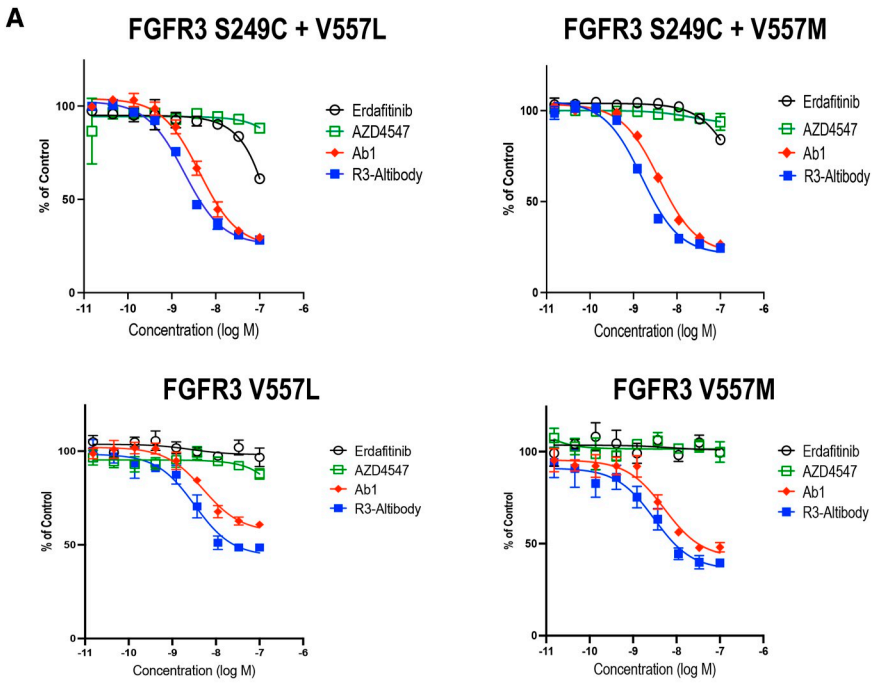

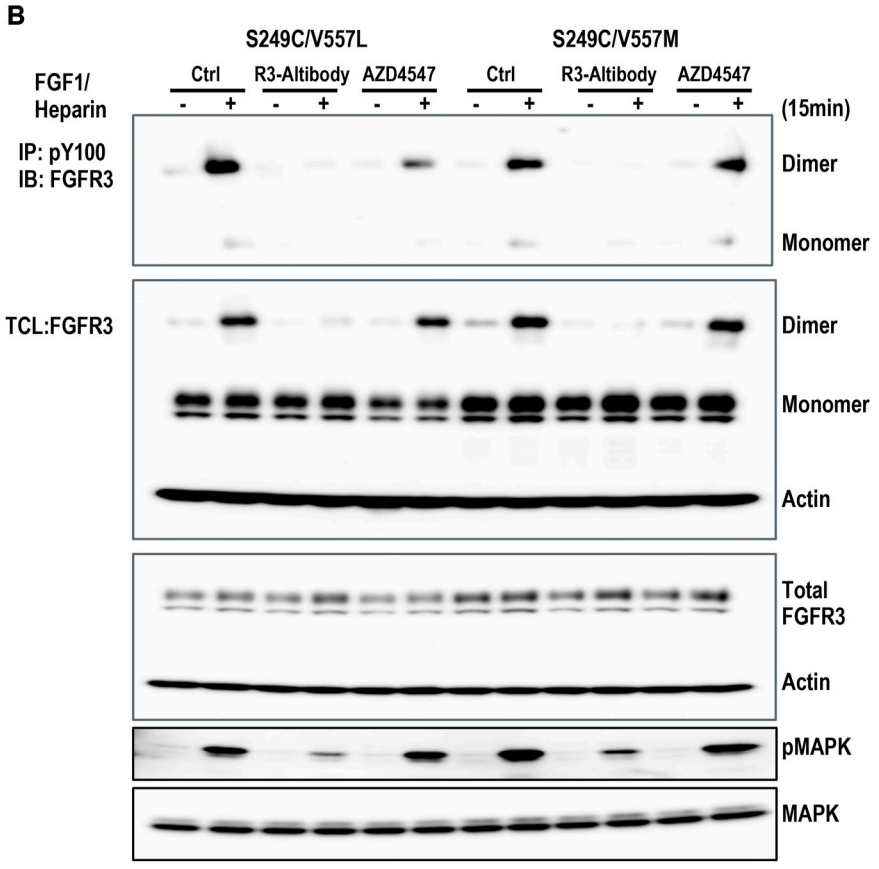

Figure 6.

R3-Altibody inhibits the function of TKI-resistant FGFR3 mutants. **A,** BaF3 cells expressing the indicated FGFR3 variants were cultured in the presence of 1 nmol/L FGF1 and 5 μg/mL heparin with increasing concentrations of the indicated antibodies (FGFR3 Ab1 or R3-Altibody) or pan-FGFR TKIs (erdafitinib, AZD4547). Cell viability was assessed after 72 hours incubation. Cell viability is expressed as percentage of untreated control and plotted as mean ± SEM. Assays were performed in triplicates. **B,** BaF3 cells expressing the indicated FGFR3 variants were serum starved overnight and treated with 100 nmol/L of R3-Altibody or AZD4547 for 6 hours, followed by stimulation with 100 nmol/L FGF1 and 10 μg/mL heparin for 15 minutes. Top, cell lysates were subjected to immunoprecipitation with antiphosphotyrosine antibody, followed by nonreducing SDS-PAGE and Western blotting to determine the levels of phosphorylated FGFR3 dimer and monomer . Middle, total cell lysates (TCL) were analyzed by nonreducing SDS-PAGE and Western blot to determine the total levels of FGFR3 dimer and monomer. Bottom, total cell lysates were analyzed under reducing conditions to determine levels of total FGFR3, actin, pMAPK, and total MAPK .

mutations (e.g., S249C) create an unpaired cysteine that drives dimerization independently of FGF ligand stimulation (10, 14). Our studies revealed that FGFR3 S249C does, however, depend on heparin for dimerization. Cell surface heparan sulfate proteoglycan (HSPG) is essential for the signaling of both paracrine and endocrine FGFs (19, 20). In normal cells, HSPG engages FGFRs and promotes the assembly of FGF/FGFR complexes (19–21). Interestingly, the expression of the FGFR3 S249C mutant in cells that lack endogenous heparan sulfate resulted in very inefficient formation of FGFR3 covalent dimers. Exogenous heparin was able to rapidly (within 15 minutes) induce covalent dimer formation (**Fig. 6B**), suggesting that heparin binding brings receptor monomers in close proximity, thereby facilitating disulfide bond formation. Thus, HSPG-induced receptor dimerization is necessary for both physiological and pathological FGFR3 signaling.

FGFR-directed TKIs have shown significant clinical activity in MIBC patients harboring FGFR3 alterations, thereby improving OS versus chemotherapy (8). However, these agents are associated with significant toxicities, which lead to frequent dose modifications (4, 7, 9) that likely limit overall clinical benefit. For instance, the FDA-approved TKI erdafitinib inhibits tyrosine kinase activity of FGFR1–4 with low nanomolar IC_{50} (1.2, 2.5, 3, and 5.7 nmol/L, respectively; ref. 22) and is associated with hyperphosphatemia, as well as gastrointestinal, nail, skin, and ocular toxicities. Hyperphosphatemia results from inhibition of FGF23/FGFR1 signaling in the kidneys, whereas gastrointestinal toxicity (diarrhea) likely results from inhibition of FGF19/FGFR4 signaling in the liver (9). Importantly, clinical experience with the FGFR3-blocking antibody vofatamab, which is a strong inhibitor of physiologic, ligand-dependent FGFR3 signaling, indicates that specific FGFR3 blockade does not lead to hyperphosphatemia, or nail or ocular toxicity (12). Although an FGFR3-selective TKI would very likely be better tolerated than the pan-FGFR TKIs, the high degree of homology of the FGFR family tyrosine kinase domains has hampered the development of such agents. Recently, however, an FGFR-3–selective inhibitor (LOXO-435) has been disclosed (23) and is currently in a Phase 1 clinical trial.

Although erdafitinib improves OS versus chemotherapy in FGFR3-altered urothelial carcinoma patients, acquired resistance limits the clinical benefit (median duration of response ~6 months, median progression-free survival of 5.5 months; ref. 7). Resistance to TKIs typically occurs via activation of compensatory signaling pathways or through secondary mutations in the target itself, which limits drug binding. *In vitro* selection of TKI-resistant FGFR3-driven cells first demonstrated that alteration of the gatekeeper residue (V555) in the FGFR3 kinase domain can mediate drug resistance (18). Clinical studies confirm that secondary mutations in the FGFR3 kinase domain are among the genetic alterations that can be detected in bladder cancers that escape from FGFR TKI treatment (17). Although signaling through the PI3K pathway seems to be a common driver of resistance, FGFR3 kinase domain mutations are detectable in ~35% of a small cohort of urothelial cancers at progression on TKI (17). Given these findings, the ability to inhibit the function of FGFR3 S249C plus V555M/L double mutants is a very important feature of our R3-Altibody.

These considerations provide a rationale to develop a potent and selective FGFR3-blocking antibody. Although the FGFR3 antibody R3Mab (later known as B-701 or vofatamab) potently blocks ligand-dependent activation of wild-type FGFR3, its efficacy in FGFR3-altered urothelial carcinoma cell models is modest (10). We show here that R3-Altibody is much more effective than our version of vofatamab in two FGFR3-driven urothelial carcinoma cell models. Thus, the limited efficacy of vofatamab in FGFR3-altered urothelial carcinoma patients likely reflects its relatively weak effect on signaling by oncogenic FGFR3 rather than a general limitation of FGFR3-blocking antibodies. In summary, the ability of our FGFR3×FGFR3 bispecific antibody to potently inhibit multiple FGFR3 oncogenic variants, including TKI-resistant variants, suggests the possibility that such an agent could provide clinical benefit to bladder cancer patients.

Authors' Disclosures

Y. Yang, A.N Suhasini, M. Rosconi, Y. Li, D. Dudgeon, A. Rafique, S. Bhosle, P. Krueger, E. Ullman, W. Olson, Y. Shen, and C. Daly report a pending patent for the work relating to this publication to Regeneron Pharmaceuticals. Regeneron Pharmaceuticals supported research and publication of this work. All authors are employee of Regeneron Pharmaceuticals. No disclosures were reported by the other authors.

Authors' Contributions

Y. Yang: Conceptualization, formal analysis, supervision, validation, investigation, visualization, methodology, writing–original draft, project administration, writing–review and editing. **A.N. Suhasini:** Resources, supervision, validation, investigation, visualization, writing–review and editing. **Z. Jiang:** Formal analysis, validation, investigation, visualization, writing–review and editing. **N. Liu:** Formal analysis, validation, investigation, visualization, writing–review and editing. **M. Rosconi:** Formal analysis, supervision, writing–review and editing. **B. Zhang:** Formal analysis, investigation, visualization, methodology, writing–review and editing. **Y. Li:** Supervision, writing–review and editing. **D. Dudgeon:** Supervision, validation, investigation, visualization, writing–review and editing. **C. Seong:** Formal analysis, validation, investigation, visualization, writing–review and editing. **S. Kim:** Investigation. **A. Rafique:** Formal analysis, validation, investigation, visualization, writing–review and editing. **T. Huang:** Resources, supervision, writing–review and editing. **S. Bhosle:** Formal analysis, validation, investigation, visualization, writing–review and editing. **P. Krueger:** Formal analysis, supervision, writing–review and editing. **E. Ullman:** Supervision, writing–review and editing. **W. Olson:** Resources, supervision, writing–review and editing. **J.C. Lin:** Supervision, writing–review and editing. **Y. Shen:** Conceptualization, resources, supervision, visualization, project administration, writing–review and editing. **C. Daly:** Conceptualization, resources, supervision, writing–original draft, project administration, writing–review and editing.

Note

Supplementary data for this article are available at Cancer Research Online (http://cancerres.aacrjournals.org/).

Received October 13, 2023; revised March 7, 2024; accepted April 11, 2024; published first July 2, 2024.

References

1. Cappellen D, De Oliveira C, Ricol D, de Medina S, Bourdin J, Sastre-Garau X, et al. Frequent activating mutations of FGFR3 in human bladder and cervix carcinomas. Nat Genet 1999;23:18–20.

2. Pietzak EJ, Bagrodia A, Cha EK, Drill EN, Iyer G, Isharwal S, et al. Next-generation sequencing of nonmuscle invasive bladder cancer reveals potential biomarkers and rational therapeutic targets. Eur Urol 2017;72:952–9.

3. Kamoun A, de Reynies A, Allory Y, Sjodahl G, Robertson AG, Seiler R, et al. A consensus molecular classification of muscle-invasive bladder cancer. Eur Urol 2020;77:420–33.
4. Loriot Y, Necchi A, Park SH, Garcia-Donas J, Huddart R, Burgess E, et al. Erdafitinib in locally advanced or metastatic urothelial carcinoma. N Engl J Med 2019;381:338–48.
5. Pal SK, Rosenberg JE, Hoffman-Censits JH, Berger R, Quinn DI, Galsky MD, et al. Efficacy of BGJ398, a fibroblast growth factor receptor 1 to 3 inhibitor, in patients with previously treated advanced urothelial carcinoma with FGFR3 alterations. Cancer Discov 2018;8:812–21.
6. Gao Q, Liang WW, Foltz SM, Mutharasu G, Jayasinghe RG, Cao S, et al. Driver fusions and their implications in the development and treatment of human cancers. Cell Rep 2018;23:227–38.e223.
7. Siefker-Radtke AO, Necchi A, Park SH, Garcia-Donas J, Huddart RA, Burgess EF, et al. Efficacy and safety of erdafitinib in patients with locally advanced or metastatic urothelial carcinoma: long-term follow-up of a phase 2 study. Lancet Oncol 2022;23:248–58.
8. Loriot Y, Matsubara N, Park SH, Huddart RA, Burgess EF, Houede N, et al. Phase 3 THOR study: results of erdafitinib (erda) versus chemotherapy (chemo) in patients (pts) with advanced or metastatic urothelial cancer (mUC) with select fibroblast growth factor receptor alterations (*FGFRalt*). J Clin Oncol 2023;41:LBA4619.
9. Siefker-Radtke AO, Necchi A, Park SH, Garcia-Donas J, Huddart RA, Burgess EF, et al. Management of fibroblast growth factor inhibitor treatment-emergent adverse events of interest in patients with locally advanced or metastatic urothelial carcinoma. Eur Urol Open Sci 2023;50:1–9.
10. Qing J, Du X, Chen Y, Chan P, Li H, Wu P, et al. Antibody-based targeting of FGFR3 in bladder carcinoma and t(4;14)-positive multiple myeloma in mice. J Clin Invest 2009;119:1216–29.
11. Necchi A, Castellano D, Mellado B, Pang S, Urun Y, Park SH, et al. Fierce-21: phase II study of vofatmab (B-701), a selective inhibitor of FGFR3, as salvage therapy in metastatic urothelial carcinoma (mUC). J Clin Oncol 2019;37:409.
12. Siefker-Radtke AO, Currie G, Abella E, Vaena DA, Kalebasty AR, Curigliano G, et al. FIERCE-22: clinical activity of vofatamab (V) a FGFR3 selective inhibitor in combination with pembrolizumab (P) in WT metastatic urothelial carcinoma, preliminary analysis. J Clin Oncol 2019;37:4511.
13. Murphy AJ, Macdonald LE, Stevens S, Karow M, Dore AT, Pobursky K, et al. Mice with megabase humanization of their immunoglobulin genes generate antibodies as efficiently as normal mice. Proc Natl Acad Sci U S A 2014;111:5153–8.
14. di Martino E, L'Hote CG, Kennedy W, Tomlinson DC, Knowles MA. Mutant fibroblast growth factor receptor 3 induces intracellular signaling and cellular transformation in a cell type- and mutation-specific manner. Oncogene 2009;28:4306–16.
15. Du X, Lin BC, Wang QR, Li H, Ingalla E, Tien J, et al. MMP-1 and Pro-MMP-10 as potential urinary pharmacodynamic biomarkers of FGFR3-targeted therapy in patients with bladder cancer. Clin Cancer Res 2014;20:6324–35.
16. Herrera-Abreu MT, Pearson A, Campbell J, Shnyder SD, Knowles MA, Ashworth A, et al. Parallel RNA interference screens identify EGFR activation as an escape mechanism in FGFR3-mutant cancer. Cancer Discov 2013;3:1058–71.
17. Facchinetti F, Hollebecque A, Braye F, Vasseur D, Pradat Y, Bahleda R, et al. Resistance to selective FGFR inhibitors in FGFR-driven urothelial cancer. Cancer Discov 2023;13:1998–2011.
18. Chell V, Balmanno K, Little AS, Wilson M, Andrews S, Blockley L, et al. Tumour cell responses to new fibroblast growth factor receptor tyrosine kinase inhibitors and identification of a gatekeeper mutation in FGFR3 as a mechanism of acquired resistance. Oncogene 2013;32:3059–70.
19. Schlessinger J, Plotnikov AN, Ibrahimi OA, Eliseenkova AV, Yeh BK, Yayon A, et al. Crystal structure of a ternary FGF-FGFR-heparin complex reveals a dual role for heparin in FGFR binding and dimerization. Mol Cell 2000;6:743–50.
20. Chen L, Fu L, Sun J, Huang Z, Fang M, Zinkle A, et al. Structural basis for FGF hormone signalling. Nature 2023;618:862–70.
21. An SJ, Mohanty J, Tome F, Suzuki Y, Lax I, Schlessinger J. Heparin is essential for optimal cell signaling by FGF21 and for regulation of betaKlotho cellular stability. Proc Natl Acad Sci U S A 2023;120:e2219128120.
22. Perera TPS, Jovcheva E, Mevellec L, Vialard J, De Lange D, Verhulst T, et al. Discovery and pharmacological characterization of JNJ-42756493 (erdafitinib), a functionally selective small-molecule FGFR family inhibitor. Mol Cancer Ther 2017;16:1010–20.
23. Ballard J, Kercher T, Abraham D, Brecht R, Brooks N, Buckles T, et al. Abstract P141: Preclinical characterization of LOX-24350, a highly potent and isoform-selective FGFR3 inhibitor. Mol Cancer Ther 2021;20(Suppl 12):P141.